









# Bipolar Waveform Synthesis With an Optically Driven Josephson Arbitrary Waveform Synthesizer

Justus A. Brevik , Dahyeon Lee , Anna E. Fox , *Senior Member, IEEE*, Yiwei Peng , Akim A. Babenko, Joe C. Campbell , *Life Fellow, IEEE*, Paul D. Dresselhaus , Franklyn Quinlan , *Senior Member, IEEE*, and Samuel P. Benz , *Fellow, IEEE*

**Abstract**—An array of Josephson junctions (JJs) was driven with photonically generated current pulses to synthesize a high-fidelity 1 kHz bipolar voltage waveform with a quantum-based amplitude that can be directly related to fundamental constants. A photodiode capable of producing high average photocurrent was used to generate large-amplitude current pulses that were ac-coupled to a JJ array. The resulting bipolar current pulses have enabled the first demonstration of quantum-based bipolar waveform synthesis with an optical drive. We measured the quantum locking range with respect to several operating parameters, including 1.2 mA with respect to a dc bias current applied to the array, confirming the robust synthesis of bipolar waveforms.

**Index Terms**—Cryogenic photonic links, Josephson arbitrary waveform synthesizer, Josephson junction (JJ) arrays, photodiodes.

## I. INTRODUCTION

THE Josephson arbitrary waveform synthesizer (JAWS) uses Josephson junctions (JJs) biased with current pulses to generate arbitrary voltage waveforms with quantum-based amplitudes traceable to fundamental constants [1]. This is achieved by exploiting the fact that when a JJ is driven with a current pulse of sufficient amplitude, it will emit a quantized voltage pulse with a time-integrated area that is exactly equal to a multiple of a magnetic flux quantum,  $\Phi_0 = \frac{h}{2e}$ , where  $h$  is the Planck constant and  $e$  is the unit of elementary charge. Arbitrary waveforms are encoded in bias pulse patterns using pulse density modulation.

Manuscript received 17 December 2021; revised 17 March 2022; accepted 23 March 2022. Date of publication 19 April 2022; date of current version 21 September 2022. This work was supported by the U.S. Government and is not subject to U.S. copyright. This article was recommended by Associate Editor I. V. Vernik. (*Corresponding author: Justus A. Brevik.*)

Justus A. Brevik, Anna E. Fox, Paul D. Dresselhaus, Franklyn Quinlan, and Samuel P. Benz are with the National Institute of Standards and Technology, Boulder, CO 80305 USA (e-mail: justus.brevik@nist.gov; anna.fox@nist.gov; paul.dresselhaus@nist.gov; franklyn.quinlan@nist.gov; samuel.benz@nist.gov).

Dahyeon Lee and Akim A. Babenko are with the National Institute of Standards and Technology, Boulder, CO 80305 USA, and also with the Department of Physics, University of Colorado Boulder, Boulder, CO 80309 USA (e-mail: Dahyeon.Lee@colorado.edu; Akim.Babenko@nist.gov).

Yiwei Peng and Joe C. Campbell are with the Department of Electrical and Computer Engineering, University of Virginia, Charlottesville, VA 22904 USA (e-mail: yp2bb@virginia.edu; jcc7s@virginia.edu).

Data is available on-line at <https://doi.org/10.18434/mds2-2630>.

Color versions of one or more figures in this article are available at <https://doi.org/10.1109/TASC.2022.3167660>.

Digital Object Identifier 10.1109/TASC.2022.3167660

When operated in the quantum locking range (QLR), where every JJ in the array generates a quantized output pulse for each input bias pulse, the synthesized waveforms have amplitudes and frequency spectra that are calculable and immune to variations in operational or environmental parameters, within certain limits. These properties make the JAWS system an ideal quantum-based standard, and it is currently in use around the world for metrology applications in the audio-frequency range [2], [3].

Recently, we have begun extending the maximum JAWS synthesis frequency to the RF and microwave range for metrology and calibration in telecommunications and quantum information applications [4]. Higher synthesis frequencies require applying more densely packed current pulses with narrower pulse widths to the JJs. This is challenging due to the limited bandwidth of electronic pulse pattern generators and the amplifiers, filters and coaxial cables that transmit the bias pulses from room temperature to the cryogenic array. Additionally, electrical pulses can broaden through dispersion during transmission to the array.

In contrast, short pulses of picosecond duration are routinely achieved in optics, and optical fibers can easily support tens of terahertz of optical bandwidth with low loss and low thermal conductivity. Using high-speed photodetectors as the interface between the optics and electronics, the bandwidth advantage of optics can be leveraged for high-bandwidth electrical pulse generation [5]. Photoconductive switches and photodiodes (PDs) have already been demonstrated up to terahertz frequencies [6], [7] and power levels of nearly 10 dBm at 100 GHz [8]. By integrating photodetectors in close proximity to cryogenic JJ circuits dispersion and distortion of the electrical pulses can be greatly reduced.

Previous efforts to drive JJ arrays with photonically generated current pulses [9] have successfully demonstrated unipolar waveform synthesis [10]–[13]. In this scheme, either strictly positive or negative current bias pulses are used to synthesize either a positive or negative polarity waveform, respectively. Bipolar synthesis, which is driven using both positive and negative current pulses, has the advantage that the maximum waveform amplitude is double that of unipolar synthesis for the same operational parameters. Additionally, the output waveform has no dc offset, which has a significant advantage in metrology applications. Photonically derived bipolar synthesis has been proposed using separate photonic links to two PDs in a balanced configuration [9], [14]–[16]. In these experiments,



cutoff frequency of  $\sim 10$  MHz to separate the high-frequency bias signals from the low-frequency biases and output voltage signal. Additionally, a bias tee was integrated in the JJ chip to voltage bias the PD through another set of taps. The bias tee was formed from the coupling capacitor of the dc block and a separate inductor on one of the tap lines. The PD was biased using a sourcemeter so that the average photocurrent could be monitored and maintained. The three pairs of taps were accessed by a six-contact dc probe module mounted to a separate piezoelectric positioner opposite the collimator positioner, as shown in Fig. 2.

A cryogenic probe station was used to provide the optical coupling and dc readout capability due to the availability of the probe station and for integration simplicity. The photonic link could be readily adapted to a simpler and less expensive liquid helium probe or a cryocooler, without the need for the positioners. An additional benefit of the probe station is the ability to easily reconfigure the setup to perform calibrated time-domain measurements of the high-frequency cryogenic PD signals in the future [18].

We used an indium-phosphide/indium-gallium-arsenide (InGaAs) modified untraveling carrier PD designed for operation at 1064 nm. The 20- $\mu\text{m}$  diameter device had a measured room-temperature RF output power of 21.7 dBm, saturation photocurrent of 95 mA, and bandwidth of 39 GHz [17]. At cryogenic temperatures, the bandgap of standard InGaAs photodetectors shifts to shorter wavelength, which greatly reduces their responsivity to 1550 nm light [19]. This bandgap shift and the availability of optical fiber amplifiers near 1  $\mu\text{m}$  led to the choice of a 1064 nm operating wavelength.

We used superconductor/normal-metal/superconductor (SNS) junctions fabricated following the same process used to produce JJ circuits for the JAWS standard reference instrument [20], [21]. The JJs were embedded in the center conductor of a CPW, with three JJs per stack and 500 stacks, for a total of 1500 series-connected junctions. A modest array of JJs was used for this preliminary demonstration, but the photonic link should be able to bias a larger array to yield larger waveform amplitudes. The junctions were measured to have an average  $I_c$  of 7.4 mA and average resistance of 4.8 m $\Omega$  at  $\sim 4$  K, for a characteristic frequency of 17 GHz.

A 1-kHz sinusoid was chosen for the synthesis demonstration. The waveform was encoded into three levels of pulses  $[-1, 0, +1]$  using second-order delta-sigma modulation (DSM) at a 30-GSa/s sampling rate or return-to-zero (RZ) rate of 15 GSa/s [22]. For this preliminary demonstration, a three-level pulse pattern was implemented as opposed to a five-level “zero-compensation” pattern [23], [24], and no ac-compensation bias was applied. The zero-compensation pattern would result in a lower residual component at the fundamental in the drive signal, which would result in less distortion of the pulse amplitude envelope incident on the JJ array after the dc block [25]. The distortion increases with increasing waveform amplitude. In the absence of an ac-compensation signal or zero-compensation the maximum waveform amplitude, while still achieving quantum-locked operation, is limited. We found that the highest delta-sigma amplitude ( $A_{\text{DSM}}$ ), that still achieved a QLR with respect to an offset bias greater than

1 mA, was  $A_{\text{DSM}} = 0.1$  at a 15-GSa/s RZ pulse-repetition frequency.

The expected quantum-based peak-to-peak voltage of the synthesized bipolar waveform can be calculated from

$$V_{pp} = 2n\Phi_0 N A_{\text{DSM}} f_{\text{PRF}} \quad (1)$$

where  $n$  is the number of junction phase rotations of  $2\pi$  that occur per bias pulse,  $N$  is the number of JJs in the array,  $f_{\text{PRF}}$  is the RZ pulse-repetition frequency, where 2 indicates the use of both pulse polarities, and  $A_{\text{DSM}} \geq 0$  but  $< 1$  for DSM stability [22]. For the choices of  $A_{\text{DSM}} = 0.1$ ,  $f_{\text{PRF}} = 15$  GHz,  $N = 1500$ , and  $n = 1$ , the expected quantum-based amplitude given by (1) was 9.3 mV pp or 3.3 mV rms.

### III. RESULTS/MEASUREMENTS

For these measurements, the synthesis goal was to obtain a minimum of 1 mA QLR with respect to dc offset current and a spurious-free dynamic range (SFDR) of at least  $-90$  dBc (decibels relative to the fundamental carrier) from the fundamental tone to the largest spurious tone. The experimental parameters that were optimized to achieve this included the PD bias, laser current bias, YDFA output power, the MZM bias point, the RF-AWG amplitude and finite impulse response (FIR) filter taps, and the RF amplifier eye-crossing adjustment and gain.

#### A. Optical Characterization

The optical parameters chosen for the waveform synthesis resulted in 37.7 mW power measured at the output of the fiber collimator and incident on the PD, with the MZM biased for maximum output. This incident power resulted in an average photocurrent of 20.5 mA. The corresponding measured responsivity of the cryogenic PD was thus 0.54 A/W. During waveform synthesis, the MZM bias was optimized near the quadrature point, which resulted in a 10.7-mA average photocurrent at a PD bias of  $-3.8$  V.

We estimated the current bias pulse amplitude and width produced by the cryogenic PD by measuring a similar PD in a room-temperature optical setup. The room-temperature PD was measured using a sampling scope with a 50- $\Omega$  input impedance. With the same optical settings used during waveform synthesis and accounting for the difference in total responsivity of the links, we measured a current bias pulse amplitude of  $\pm 8.5$  mA and pulsewidth of  $\sim 62$  ps. The latter was consistent with the measured width of the electrical pulses from the RF-AWG and amplifier, and was due to the optimal FIR filter taps and analog bandwidth of the RF-AWG. It was not limited by the PD bandwidth.

We performed additional cryogenic measurements of the maximum average photocurrent by increasing the YDFA output power. In part, we wanted to test the feasibility of biasing multiple arrays with a single PD using on-chip power dividers [26], [27]. We selected a conservative cutoff of 42 mW incident on the PD to avoid the risk of thermally damaging it, since the heatsinking of the PD during cryogenic operation had not been characterized. This incident power yielded an average photocurrent of 22.7 mA. With the MZM biased at a quadrature point, so



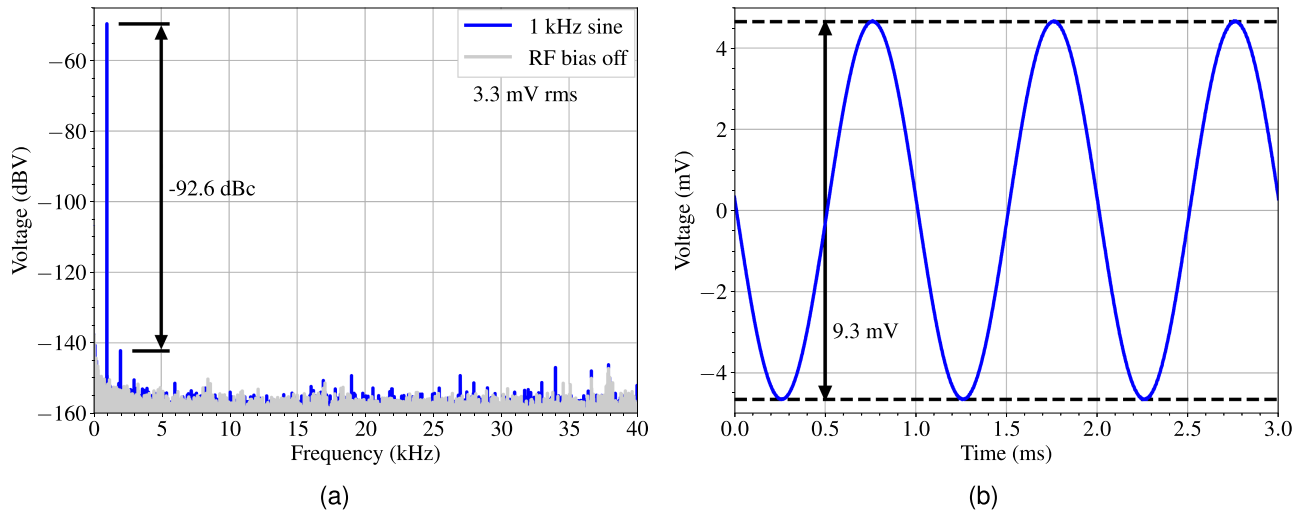


Fig. 3. Digitally sampled measurements of a 1-kHz bipolar sinusoid. The digitizer was set to a 1 megasample-per-second sampling rate, 1 M $\Omega$  input impedance, and  $\pm 1$  V input range. (a) Spectra for the synthesis of a 1-kHz sinusoid, “1 kHz sine,” and with the RF modulation to the MZM turned OFF, “RF bias OFF.” These spectra were acquired with no averaging, and a resolution bandwidth of 5 Hz. The measured rms amplitude of the synthesized sinusoid was 3.3 mV. The spurious free dynamic range between the 1-kHz fundamental and the 2-kHz harmonic was measured to be  $-92.6$  dBc (decibels relative to the fundamental carrier). (b) Timestream showing three periods of the output waveform with no averaging, with a measured peak-to-peak amplitude of 9.3 mV.

that the average photocurrent is half this value, peak pulse amplitudes of  $\pm 11.4$  mA should be possible. Assuming a  $\sqrt{2}$  current division for each layer of divider and the same  $I_c$  and  $\pm 8.5$  mA optimal bias amplitude, a single-layer divider would require a  $\pm 12$  mA pulse amplitude or  $\geq 24$  mA peak photocurrent, and a double-layer divider would require  $\pm 17$  mA pulse amplitude or  $\geq 34$  mA peak photocurrent. The conservative power cutoff was nearly sufficient for a single-layer divider. Given that the PD had a room-temperature saturation photocurrent of 95 mA, we are optimistic that it will be able to produce pulse amplitudes sufficient to bias multiple JJ arrays using a double-layer power divider.

### B. Thermal Characterization

We assessed the loading of the cryogenic sample stage by the photonic link using two methods. First, we estimated the load from the measured optical and electrical power dissipated on the cold stage. The electrical power was estimated from the 10.7-mA average photocurrent that was maintained during synthesis and the  $-3.8$  V PD bias, to give 40.7 mW of electrical bias loading. If all of the optical power incident on the PD eventually went into dissipated heat on the sample stage, there was an additional 37.7 mW of optical loading. The total loading of the photonic link on the sample stage from the first method was estimated at  $\sim 78$  mW.

The second estimate was derived from thermal load curves and the rise in the sample stage temperature when the relevant optical and electrical signals were turned on for waveform synthesis. Load curves for the thermal link between the sample stage and 4 K stage were measured from the rise in temperature of the sample stage at different applied heater power levels. The load curves indicated a  $\sim 76$ -mW load based on the sample stage temperature increase.

The two estimates are in agreement, and indicate a total thermal load of  $\sim 77$  mW. The cryogenic probe station has  $\sim 1.5$  W of cooling power at 4.2 K, so this load did not pose a problem. However, it could be problematic for cryocoolers with lower cooling power. This issue could be mitigated by mounting an appropriately packaged PD on a thermal stage with higher cooling capacity and then connecting the PD output to the JJ array using short coaxial cabling. We also note that the thermal effects from applying  $\sim 77$  mW in close proximity to the JJ array did not appear to impact the waveform synthesis.

### C. Bipolar Waveform Synthesis

The synthesized 1 kHz bipolar sinusoid is shown in Fig. 3. Two hundred periods of the output waveform were measured using a digitizer, set to a 1 megasample-per-second sampling rate and 1 M $\Omega$  input impedance, which was connected to the low-pass filtered lines  $V_{out}$ . During this measurement, the current bias applied to the array using the filtered lines  $I_{dc}$  was set to 0 A, though any value within the QLR would have yielded the same result. The first three periods of the measured time-domain bipolar waveform are shown in Fig. 3(b), with no averaging applied to the timestream. The measured waveform amplitude was 9.3 mV pp, in agreement with the predicted voltage.

The frequency-domain representation of the measurement is shown as “1 kHz sine” in Fig. 3(a), in units of dBV (decibels relative to 1 V). We acquired an additional spectrum with the output of the RF-AWG to the MZM turned OFF, labeled “RF bias OFF,” to demonstrate the digitizer noise floor and spurious signal generation without RF modulation. The amplitude of the synthesized 1 kHz tone was  $-49.7$  dBV, equivalent to an rms amplitude of 3.3 mV. The next highest spur in the synthesized spectrum occurred at the 2-kHz second harmonic with an amplitude of approximately  $-142$  dBV. The measured SFDR was  $-92.6$  dBc

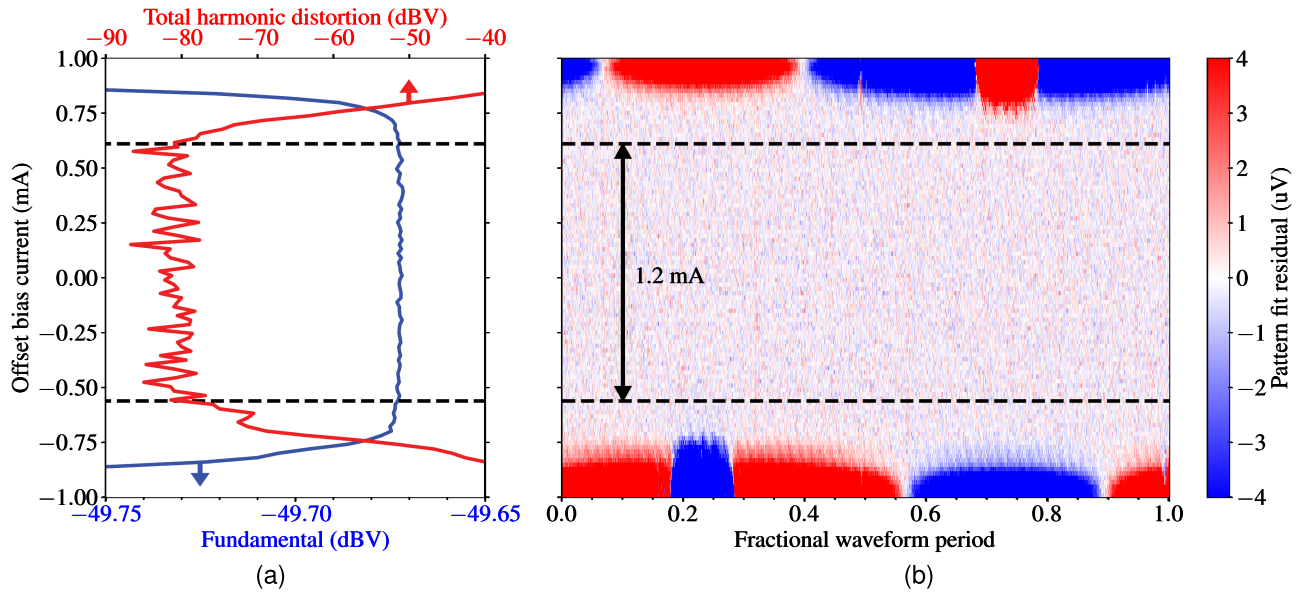


Fig. 4. Quantum locking range (QLR) of the 1-kHz bipolar sinusoid with respect to an offset bias current. (a) Fundamental 1 kHz tone and the total harmonic distortion (THD) on the x-axis versus the amplitude of a 5-Hz triangular bias waveform (y-axis). (b) Same data after the dc and fundamental components were removed and the residual was plotted as the fraction of the 1-ms waveform period (x-axis) versus offset bias amplitude (y-axis). The horizontal lines indicate the 1.2-mA region where the fundamental and THD (left) and pattern residual (right) were independent of the offset current.

relative to the 1-kHz fundamental tone and the measured total harmonic distortion (THD) was  $-91.4$  dBV, illustrating that a high-fidelity signal was produced by the photonic driven JJs. In comparison, the electrically driven JAWS systems generally have an SFDR of  $-115$  dBc or better, which is limited by the linearity of the digitizer.

We attribute the degradation in the SFDR for the optically driven system to the nonlinear response of the optics and electro-optics, with the dominant contribution coming from the MZM. The nonlinear distortion caused by MZMs is a well-known characteristic of analog photonic links. Several linearization techniques have been developed to counteract this, including signal predistortion, balancing photodiode and modulator nonlinearities, and dual-parallel MZMs [28], [29]. We believe such techniques can be applied to this bias scheme to ultimately improve the SFDR.

#### D. Quantum Locking Range Measurements

In addition to confirming the synthesized waveform amplitude agreed with the quantum-based expectation, we also measured the QLR of the synthesis with respect to a dc bias current, as shown in Fig. 4. This bias added an additional dc current to the ac-coupled bias pulses at the JJ array. As the offset increased to a certain maximum positive or negative value, the current bias pulses no longer fell within the range that ensured that each JJ in the array produced a single quantized voltage pulse for every bias pulse. These extrema represent the edges of the QLR with respect to dc bias current. We measured a 1.2-mA quantum locking range for this experiment, thereby confirming the successful quantum-based operation of the optically biased JAWS system.

The QLR measurement in Fig. 4 follows the visualization technique introduced in [26]. A 5-Hz triangular bias was applied to  $I_{dc}$  while 200 periods of the synthesized waveform were digitized. Fig. 4(a) shows plots of both the amplitude of the 1-kHz fundamental tone and the THD in dBV (x-axis) versus the amplitude of the triangular bias waveform (y-axis). Over a range of bias current the fundamental and THD remain relatively constant. At the edges of the QLR the fundamental amplitude begins to decrease and the THD begins to increase.

Note the floor of the THD plot in Fig. 4(a) is approximately  $-80$  dBV, which is higher than the  $-91.4$  dBV for the THD of the spectrum in Fig. 3(a). Only one waveform period is used to calculate each pair of THD and fundamental points in Fig. 4(a) to keep the instantaneous offset bias and the synthesized spectrum relatively static in the presence of the 5-Hz triangular bias. The lower sample size compared to the 200-period acquisition used in Fig. 3(a) increases the noise floor of the THD calculation.

Another way to visualize the QLR is shown in Fig. 4(b), which is the primary tool for varying the operational parameters to optimize the QLR. The fast Fourier transform (FFT) of the synthesized waveform was calculated, the dc and 1 kHz frequency bins were set to zero, and then the inverse FFT of the result was calculated to produce a timestream with only residual signal remaining. The data were then organized so that the x-axis depicts the fraction of the 1-ms waveform period, and the y-axis depicts the corresponding offset current for the triangular bias waveform. In the vertical center of this map is a region where the residual timestream is consistent with measurement noise, indicating an offset range over which every bias pulse resulted in a single quantized output pulse for every JJ in the array. The vertical extent of this QLR, indicated by the horizontal dashed lines, was measured to be 1.2 mA.

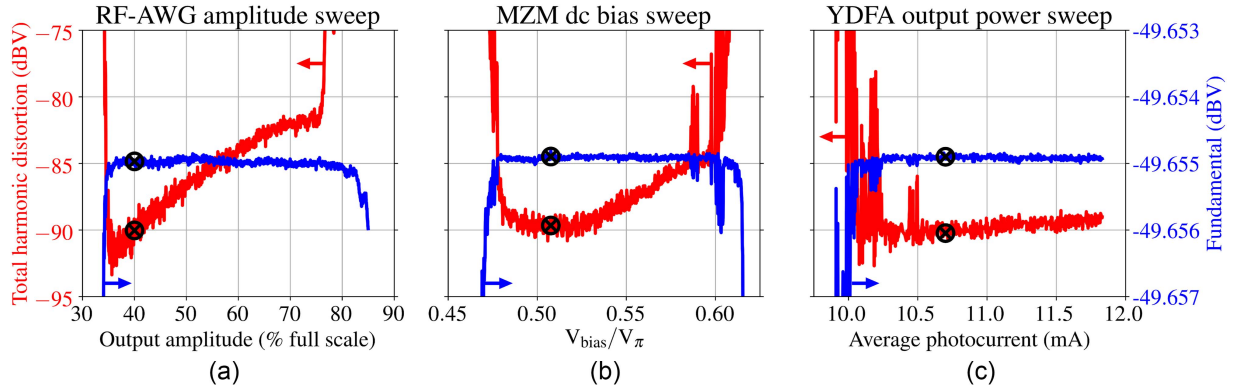


Fig. 5. Optical drive parameter sweeps. The blue plots show the response of the fundamental 1 kHz sinusoid amplitude and the red plots show the THD response. (a) Output amplitude of the RF-AWG was varied. (b) MZM dc bias voltage was varied. (c) YDFA output power was varied, which has been plotted in terms of average photocurrent. The operational points used for the waveform synthesis are indicated by the  $\otimes$  markers.

We also measured QLRs with respect to operational parameters related to the optical signal, to demonstrate the robustness of the bipolar synthesis to their variation. As shown in Fig. 5, we swept the RF-AWG amplitude, the MZM dc bias voltage, and the YDFA output power. During the sweeps, the experimental parameters were fixed at the values used for the waveform synthesis, and only one parameter was varied at a time. The spectra used for each sweep point were calculated from 200 waveform periods, so the THD plots have a noise floor equivalent to that in Fig. 3(a), as opposed to Fig. 4(a).

The plots of the fundamental tone in Fig. 5 have ranges where they do not vary with the sweep parameter. However, the THD plots clearly show variation. We attribute this to the nonlinear response of the optical components, especially the MZM, which generate harmonics of the 1-kHz tone present in the RF modulation. These low-frequency signals couple to the JJ array and add vectorially to the quantum-based synthesized signal. The harmonic amplitudes are sensitive to variations in the optical bias parameters, so they vary with the sweep and obscure the underlying flat THD response of the synthesized signal. We verified the nonlinear signal generation by measuring the output of the room-temperature PD setup. Despite the THD variation, we believe these measurements demonstrate quantum-locked operation of the source with respect to the optical parameters. We have derived the QLRs from the range between substantial excursion of the THD. We are optimistic the nonlinear response can be mitigated in future experiments and the resulting QLRs will no longer include THD variation.

Fig. 5(a) shows the QLR with respect to the RF-AWG amplitude, which has been plotted in terms of the percentage of the 1-V pp output. For this sweep, the output amplitude was varied while maintaining the average photocurrent at the optimal 10.7 mA synthesis value. The sweep varied the modulation amplitude at the MZM RF port, and therefore varied the amplitude of the current pulses generated by the PD. At the lower limit of the sweep, the bias pulse amplitude was too low to ensure proper pulse quantization by the JJs. At the upper limit the RF modulation exceeded the  $V_\pi$  of the MZM's RF port, causing the pulses to wrap the sinusoidal response curve. The synthesis remained quantum-locked between 37% and 75% of full scale. The THD varied by  $\sim 10$  dB over this range due to the

high sensitivity of the MZM nonlinearity to the RF modulation amplitude. The RF-AWG amplitude was set to 40% of full scale during waveform synthesis to minimize the THD and avoid the large THD excursion around 35%.

Fig. 5(b) shows the QLR with respect to the dc bias voltage of the MZM, which has been plotted in terms of the fractional bias with respect to the dc  $V_\pi$  of the MZM. This sweep indicated the extent to which the optimal bias point could drift while still ensuring quantum-locked operation. The synthesis remained quantum-locked between 48 and 58% of  $V_\pi$ . The THD varied by  $\sim 5$  dB over this range due to the sensitivity of the MZM nonlinearity to its bias point. The bias point was set to 51% of  $V_\pi$  during waveform synthesis to minimize the THD.

Fig. 5(c) shows the QLR with respect to the YDFA output power, which has been plotted in terms of average photocurrent. During the sweep, the MZM bias was maintained at the optimal synthesis value. The synthesis remained quantum-locked from 10.5 to 11.8 mA average photocurrent. Since the RF-AWG amplitude was maintained at the optimal synthesis value, the bias pulse amplitude also varied. As measured from the room-temperature PD setup, this photocurrent range was equivalent to a variation of the bias pulse amplitude from  $\pm 8.2$  to  $\pm 9.5$  mA. The output power was swept up to a conservative value that would ensure the PD would be safe from thermal damage. The upper limits of these ranges only indicate the bound given by that maximum setting. The actual upper bounds of the QLR exceed these values, as the THD showed no sign of an excursion.

Of the optical drive parameters that were swept, drift in the optimal MZM dc bias is the most sensitive to long-term variability and subsequently can lead to degradation of the spectral purity of the waveform synthesis. However, bias point drift minimization is relatively straightforward and can be achieved through temperature stabilization of the MZM or through active feedback control [30].

#### IV. CONCLUSION

In this article, we have driven a JJ array with a photonic link and demonstrated quantum-based bipolar waveform synthesis for the first time. Bipolar synthesis with a single photodiode was



made possible by using the ac-coupled output of a high-power photodiode operating at  $\sim 4$  K. The synthesized waveform had an amplitude of 3.3 mV rms, which agreed with the expected quantum-based amplitude. Furthermore, a quantum locking range with respect to offset bias of 1.2 mA was measured, demonstrating that the optically driven JAWS system can robustly synthesize waveforms in quantum-locked operation. Additional parameter sweeps showed quantum-locked operation with respect to several optical drive parameters, including the optical amplifier output power, the electro-optic modulator bias point, and the RF modulation amplitude. The SFDR of the synthesized spectrum was measured at  $-92.6$  dBc from the 1-kHz synthesized tone to the largest harmonic at 2 kHz, demonstrating the synthesis of a waveform with high spectral purity.

The main limitation in this preliminary optical-drive implementation was the nonlinear response of the optics and electro-optics, especially that of the electro-optic modulator. These components generated harmonic signals from the residual signal at the 1-kHz fundamental in the RF modulation, which coupled to the JJ array and added vectorially to the synthesized signal. The nonlinear signals degraded the SFDR and caused variation of the THD in measurements of the optical-parameter QLRs. The measured SFDR of  $-92.6$  dBc is sufficient for most applications, but the SFDR and THD can be improved in future experiments through the implementation of various linearization techniques developed for analog photonic links.

Furthermore, due to the high output power of the photodiode, we can reduce the nonlinear response by increasing the optical amplification and decreasing the RF modulation amplitude to the modulator. However, this will come at the expense of additional thermal loading. Additionally, the inner-outer block could be replaced with a high-pass filter to further reduce the nonlinear signals that couple to the JJ array. Finally, we plan to implement a zero-compensation pulse pattern in the next measurement run to increase the maximum  $A_{\text{DSM}}$ . Zero-compensation reduces the residual signal at the fundamental by digitally high-pass filtering the drive pattern. Reducing the residual fundamental in the RF modulation should reduce the optically generated harmonic signals that couple to the JJ array. It should also improve the frequency-dependent inductive voltage error, the so-called “feedthrough” error, which will be important to mitigate when synthesizing RF signals [24].

Extending high-fidelity waveform synthesis to higher frequencies requires increasing the pulse sampling rate, while maintaining narrow pulse widths from the photodiode. These requirements will eventually exceed the capability of electrical pattern generators. The broad bandwidth capabilities of optical pulse sources, optical fiber, and photodetectors provide a path to extend the synthesis frequencies of quantum-based waveform generation.

#### ACKNOWLEDGMENT

The authors would like to thank S. Diddams for his support and insightful comments throughout this project, N. Flowers-Jacobs for his informative discussions, M. C. Beltran, A. Sirois

for their work on the cryogenic probe station, and the National Institute of Standards and Technology Boulder Micro-fabrication Facility for fabrication expertise.

#### REFERENCES

- [1] S. P. Benz and C. A. Hamilton, “A pulse-driven programmable Josephson voltage standard,” *Appl. Phys. Lett.*, vol. 68, no. 22, pp. 3171–3173, 1996.
- [2] N. E. Flowers-Jacobs *et al.*, “Development and applications of a four-volt Josephson arbitrary waveform synthesizer,” in *Proc. IEEE Int. Superconductive Electron. Conf.*, 2019, pp. 1–2.
- [3] J. Kohlmann, “Application to Josephson voltage standards,” in *Josephson Junctions: History, Devices and Applications*. Redwood City, CA, USA: Pan Stanford Publishing, 2017, pp. 359–377.
- [4] P. F. Hopkins *et al.*, “RF waveform synthesizers with quantum-based voltage accuracy for communications metrology,” *IEEE Trans. Appl. Supercond.*, vol. 29, no. 5, pp. 1–5, Aug. 2019.
- [5] J. Nissilä *et al.*, “Driving a low critical current Josephson junction array with a mode-locked laser,” *Appl. Phys. Lett.*, vol. 119, no. 3, 2021, Art. no. 032601.
- [6] H. Ito, T. Nagatsuma, and T. Ishibashi, “Uni-traveling-carrier photodiodes for high-speed detection and broadband sensing,” in *Quantum Sens. and Nanophotonic Devices IV* vol. 6479, M. Razeghi and G. J. Brown, Eds. Bellingham, WA, USA: SPIE, 2007, pp. 150–163.
- [7] C. S. H. S. Yardimci, N. T., and M. Jarrahi, “A high-power broadband terahertz source enabled by three-dimensional light confinement in a plasmonic nanocavity,” *Sci. Rep.*, vol. 7, 2017, Art. no. 4166.
- [8] Q. Li *et al.*, “High-power flip-chip bonded photodiode with 110 GHz bandwidth,” *J. Lightw. Technol.*, vol. 34, no. 9, pp. 2139–2144, 2016.
- [9] J. M. Williams *et al.*, “The simulation and measurement of the response of Josephson junctions to optoelectronically generated short pulses,” *Supercond. Sci. Technol.*, vol. 17, no. 6, pp. 815–818, Apr. 2004.
- [10] C. Urano *et al.*, “Operation of a Josephson arbitrary waveform synthesizer with optical data input,” *Supercond. Sci. Technol.*, vol. 22, no. 11, Oct. 2009, Art. no. 114012.
- [11] O. Kieler *et al.*, “Optical pulse-drive for the pulse-driven AC Josephson voltage standard,” *IEEE Trans. Appl. Supercond.*, vol. 29, no. 5, Aug. 2019, Art. no. 1200205.
- [12] J. Ireland *et al.*, “An optoelectronic pulse drive for quantum voltage synthesizer,” *IEEE Trans. Instrum. Meas.*, vol. 68, no. 6, pp. 2066–2071, Jun. 2019.
- [13] B. Karlsen *et al.*, “Pulsation of InGaAs photodiodes in liquid helium for driving Josephson arrays in AC voltage realization,” *IEEE Trans. Appl. Supercond.*, vol. 29, no. 7, Oct. 2019, Art. no. 1200308.
- [14] B. Karlsen *et al.*, “High-speed pulsation of a cryogenically operable bipolar photodiode module for the Josephson arbitrary waveform synthesizer,” in *Proc. Conf. Precis. Electromagn. Meas.*, 2020, pp. 1–2.
- [15] J. Herick *et al.*, “Realization of an opto-electronic bias for pulse-driven Josephson voltage standards at PTB,” in *Proc. Conf. Precis. Electromagn. Meas.*, 2020, pp. 1–2.
- [16] E. Bardalen, J. Nissilä, T. Fordell, B. Karlsen, O. Kieler, and P. Ohlckers, “Bipolar photodiode module operated at 4k,” in *Proc. IEEE 8th Electron. Syst.-Integration Technol. Conf.*, 2020, pp. 1–5.
- [17] Y. Peng, K. Sun, Y. Shen, A. Beling, and J. C. Campbell, “High-power and high-linearity photodiodes at 1064 nm,” *J. Lightw. Technol.*, vol. 38, no. 17, pp. 4850–4856, 2020.
- [18] J. A. Brevik *et al.*, “Cryogenic calibration of the RF Josephson arbitrary waveform synthesizer,” in *Proc. Conf. Precis. Electromagn. Meas.*, 2020, pp. 1–2.
- [19] E. Zielinski, H. Schweizer, K. Streubel, H. Eisele, and G. Weimann, “Excitonic transitions and exciton damping processes in InGaAs/InP,” *J. Appl. Phys.*, vol. 59, no. 6, pp. 2196–2204, 1986.
- [20] A. E. Fox, P. D. Dresselhaus, A. Rüfenacht, A. Sanders, and S. P. Benz, “Junction yield analysis for 10 V programmable Josephson voltage standard devices,” *IEEE Trans. Appl. Supercond.*, vol. 25, no. 3, Jun. 2015, Art. no. 1101505.
- [21] National Institute of Standards and Technology Standard Reference Instrument. [Online]. Available: <https://www.nist.gov/sri/standard-reference-instruments/sri-6011-josephson-arbitrary-waveform-synthesizer>
- [22] G. T. S. Pavan and R. Schreier, *Understanding Delta-Sigma Data Converters*, 2nd ed. Hoboken, NJ, USA: Wiley, 2017.
- [23] K. Zhou, J. Qu, and S. P. Benz, “Zero-compensation method and reduced inductive voltage error for the AC Josephson voltage standard,” *IEEE Trans. Appl. Supercond.*, vol. 25, no. 5, Oct. 2015, Art. no. 1400806.

- [24] J. A. Brevik, N. E. Flowers-Jacobs, A. E. Fox, E. B. Golden, P. D. Dresselhaus, and S. P. Benz, "Josephson arbitrary waveform synthesis with multilevel pulse biasing," *IEEE Trans. Appl. Supercond.*, vol. 27, no. 3, Apr. 2017, Art. no. 1301707.
- [25] S. P. Benz and S. B. Waltman, "Pulse-bias electronics and techniques for a Josephson arbitrary waveform synthesizer," *IEEE Trans. Appl. Supercond.*, vol. 24, no. 6, Dec. 2014, Art. no. 1400107.
- [26] N. E. Flowers-Jacobs *et al.*, "Two-volt Josephson arbitrary waveform synthesizer using Wilkinson dividers," *IEEE Trans. Appl. Supercond.*, vol. 26, no. 6, Sep. 2016, Art. no. 1400207.
- [27] N. E. Flowers-Jacobs, S. B. Waltman, A. E. Fox, P. D. Dresselhaus, and S. P. Benz, "Josephson arbitrary waveform synthesizer with two layers of Wilkinson dividers and an FIR filter," *IEEE Trans. Appl. Supercond.*, vol. 26, no. 6, Sep. 2016, Art. no. 1400307.
- [28] M. N. Hutchinson, J. M. Singley, V. J. Urick, S. R. Harmon, J. D. McKinney, and N. J. Frigo, "Mitigation of photodiode induced even-order distortion in photonic links with predistortion modulation," *J. Lightw. Technol.*, vol. 32, no. 20, pp. 3885–3892, 2014.
- [29] V. J. Urick, J. D. Mckinney, and K. J. Williams, *Distortion in Fiber Optic Links*. Hoboken, NJ, USA: Wiley, 2015, ch. 4, pp. 124–165. [Online]. Available: <https://onlinelibrary.wiley.com/doi/abs/10.1002/9781119029816.ch4>
- [30] J. P. Salvestrini, L. Guilbert, M. Fontana, M. Abarkan, and S. Gille, "Analysis and control of the dc drift in LiNbO<sub>3</sub>-based Mach-Zehnder modulators," *J. Lightw. Technol.*, vol. 29, no. 10, pp. 1522–1534, 2011.